Cover

# A waste-to-resource strategy to fabricate highly porous whisker-structured mullite ceramic membrane for simulated oil-in-water emulsion wastewater treatment

Mingliang Chen[a,b], Li Zhu[a,b], Yingchao Dong[a,b,*], Lingling Li[a,b,c], Jing Liu[a,b,c]

a. CAS Key Laboratory of Urban Pollutant Conversion, Institute of Urban Environment, Chinese Academy of Sciences, P.R. China
b. Ningbo Urban Environment Observation and Research Station—NUEORS, Chinese Academy of Sciences, P.R. China
c. School of Chemistry and Chemical Engineering, South China University of Technology, Guangzhou, P.R. China

The manuscript has 32 pages, 1 table, and 7 figures.

The Supporting Information has 12 pages, 2 tables, and 9 figures.

# Supporting information

## Characterization of starting materials

The chemical compositions of fly ash and bauxite characterized by semiquantitative X-ray fluorescence spectrum analysis are listed in Tab. S1. The fly ash is mainly composed of $SiO_2$ (56.39 wt. %) and $Al_2O_3$ (32.75 wt. %), and contains a small amount of other metal oxides (3.61 wt. % $Fe_2O_3$, 1.33 wt. % $TiO_2$, 1.62 wt. % CaO). While the main components of bauxite are $Al_2O_3$ (66.87 wt. %), $SiO_2$ (9.19 wt. %) and $Fe_2O_3$ (5.55 wt. %). Fig. S1 displays the particle size distributions of fly ash and bauxite. As shown in Fig. S1a, the particle size of fly ash mainly ranges from 1.06 to 44.63 μm ($d_{10}$-$d_{90}$) with an average value (D50) of 11.94 μm, while in Fig. S1b, the D50 of bauxite is 5.66 μm, with most particles in the range of 0.5-14.62 μm ($d_{10}$-$d_{90}$).

Fig. S2 displays the XRD patterns of fly ash and natural bauxite. Mullite ($3Al_2O_3 \cdot 2SiO_2$, PDF#79-1455) and quartz (α-$SiO_2$, PDF#89-8936) are detected as the major crystalline phases in the fly ash. As to natural bauxite, the major phases are diaspore (AlO(OH), PDF#87-0705) and kaolinite ($3Al_2O_3 \cdot 2SiO_2 \cdot 2H_2O$, PDF#78-2109).

**Table S1 Chemical compositions of raw materials measured by XRF**

| Materials | Chemical composition (wt. %) | | | | | | | | | | |
|---|---|---|---|---|---|---|---|---|---|---|---|
| | $Al_2O_3$ | $SiO_2$ | $TiO_2$ | $Fe_2O_3$ | MgO | CaO | $K_2O$ | $SO_3$ | $P_2O_5$ | $Na_2O$ | LOI* |
| Fly ash | 32.75 | 56.39 | 1.33 | 3.61 | 0.97 | 1.62 | 0.89 | 0.18 | 0.46 | 0.03 | 1.77 |
| bauxite | 66.87 | 9.19 | 2.92 | 5.55 | 0.08 | 0.77 | 0.44 | 0.13 | 0.32 | 0.14 | 13.59 |

*LOI refers to the loss on ignition

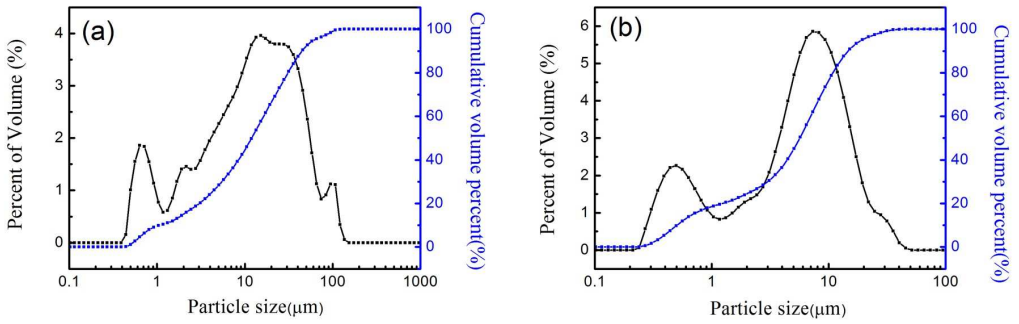


**Fig. S1 Particle size distributions of (a) coal fly ash and (b) natural bauxite.**

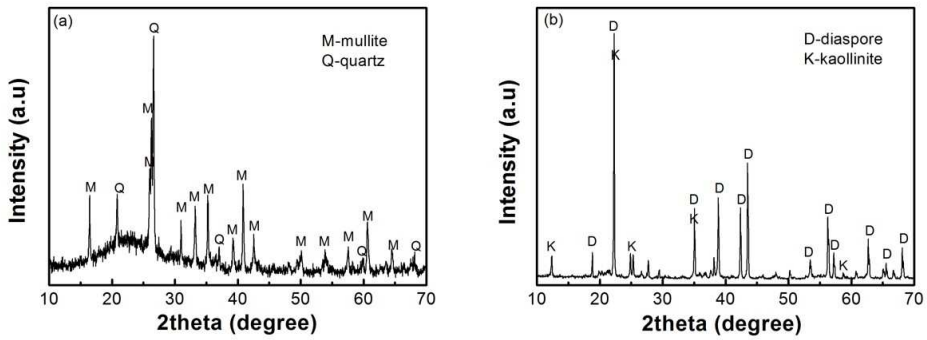


**Fig. S2 XRD patterns of two starting materials: (a) waste fly ash and (b) natural bauxite.**

## Preparation of membrane green compacts

The green compacts in our work were made by a uniaxial dry pressing method. The mixture of fly ash and bauxite powders was first wet milled for 20 minutes in an alumina mortar using alumina pestle for sufficient mixing, then the slurries were completely dried at 100°C for 2~3 h. After complete drying, organic binder PVA-1750 solution (5 wt. %) was added and uniformly mixed with the milled mixtures and dried at 100°C for 2~3 h again. At last, the green compacts (20 mm in diameter and 1–2 mm in thickness) were produced by uniaxial dry pressing of the powders at a pressure of 6 MPa. The green disc-shaped membranes were placed in a closed alumina crucible and sintered in an electrically heated muffle furnace in air for 2h at various final temperatures ranging from 1100 to 1500 °C. The punching machine used to fabricate the green compacts are shown in Fig. S3.

Fig. S3 The press machine used to fabricate membrane green compacts.

**RIR analysis method**

Relative intensity ratio (RIR) method is one of the simplest and quickest ways to quantify phase content using X-ray diffraction patterns [1,2]. In this work, RIR method was used for phase quantitation. For this method, the variation of peak intensities with concentration is considered to be not linear and the former is derived by standards. The standards can either be used either internally or externally. For the internal standard method, a certain amount of a known component is mixed with the sample to be tested. Several reference samples are prepared in this manner by varying the mass ratios of the two components (standard and sample). For external standard method, different mixtures of pure mineral phases with various weight fractions, which are known to be present in the unknown samples, are used as standards. These mixtures are tested and X-ray diffraction patterns are obtained for each of them. The peak intensity of a major reflecting line of the known minerals is monitored across varying concentrations. A calibration graph is prepared by plotting peak intensity ratios of minerals in prepared standards against their weight fractions.

The general definition of the RIR for phase β to reference phase α is given by:

$$\mathrm{RIR}_{\alpha,\beta} = \left(\frac{I_{\mathrm{hkl}\alpha}}{I_{\mathrm{hkl}\beta}}\right)\left(\frac{X_\beta}{X_\alpha}\right)$$

where $I$ is the intensity and $X$ is the weight fraction. Rearranging the above equation:

$$X_\beta = \left(\frac{I_{\mathrm{hkl}\beta}}{I_{\mathrm{hkl}\alpha}}\right)\left(\frac{X_\alpha}{\mathrm{RIR}_{\alpha,\beta}}\right)$$

The RIR value may be obtained by determination of the slope of the standard calibration plot or from other RIR values by:

$$\mathrm{RIR}_{\alpha,\beta} = \frac{\mathrm{RIR}_{\alpha,\gamma}}{\mathrm{RIR}_{\beta,\gamma}}$$

If a mixture is composed of known phases each with known values of RIR, the fractions of all the phases must add to 1. This allows the following summation equation to be written:

$$X_i = (I_{\mathrm{hkl}i})(K_{i,n})\left[\frac{1}{\sum_{j=1}^{m}(I_{\mathrm{hkl}'j})(K_{j,n})}\right]$$

where $Xi$ is the unknown weight fraction of phase $i$ in the sample, $Ki,n$ and $Kj,n$ are the RIR value for diffraction line $n$ of phase $i$ and $j$, $Ii,n$ and $Ij,n$ are the integrated intensity of diffraction line $n$ of phase $i$ and $j$ respectively, and $m$ is the number of phases in the mixture. This is known as the normalized RIR method.

In this work, the values of RIR and I for each phase were obtained by the software Jade 6.0. Thus, each phase content was calculated through this method. Usually, RIR method is a semi-quantitative way to determine each phase content. Hillier reported that RIR analysis gave the results with an accuracy of within ~±3 wt.% at a confidence level of 95%.

**Sintering behavior of membrane green compacts**

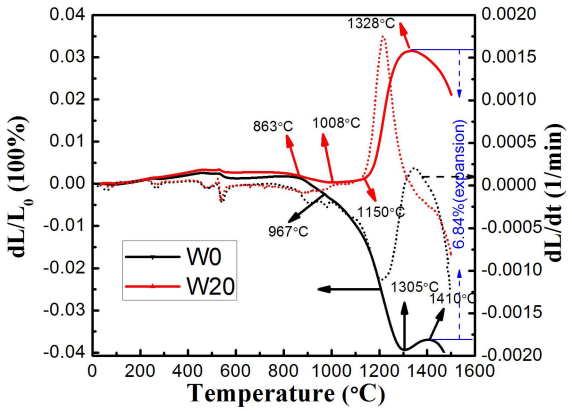


**Fig. S4 Linear shrinkage ($dL/L_0$) and differential linear shrinkage (dL/dt) between room temperature (20 ˚C) and 1500 ˚C of W0 and W20 green membranes.**

The dynamic sintering curves of the green rectangular bar of mullite ceramic membranes are shown in Fig. S4. For W0 samples, the sintering behavior can be divided into three stages at high temperature (above 800 ˚C). In the first stage, a huge densification behavior (3.7 % shrinkage) happens at 967 ˚C and extends to 1305 ˚C. Then a slight volume expansion process (0.258 % expansion) is observed with increasing temperature from 1305 to 1410 ˚C, which can be attributed to the anisotropic growth of mullite crystals during this process. Above 1410 ˚C, a re-densification process occurs and the sample shrinks again duo to a liquid phase sintering.

However, as compared to W0, the W20 sample shows a very different dynamic sintering behavior. From 863 to 1008 ˚C, only a very minor densification with a shrinkage of 0.19 % is observed, followed by a very small expansion process from 1008 ˚C to 1150 ˚C. Then a huge self-expansion process occurs between 1150 and 1328 ˚C with an expansion rate as high as 2.984 %, which is much higher than that of W0 (only 0.258%). This improved expansion ratio of 6.84 % caused by addition of 20 wt. % $WO_3$ is much higher than those by addition of other additives, such as $V_2O_5$ [3] (5 wt. % $V_2O_5$+4 wt. % $AlF_3$, 3.92 % expansion ratio), MgO [4]. Above 1328 ˚C, the sample shows a re-shrinkage due to the liquid sintering reaction.

By comparison, it can be concluded that the mullite formation temperature could be reduced significantly with the addition of 20 wt. % $WO_3$ and its expansion ratio of W20 is 6.84 % greater than W0.

**Shrinkage and open porosity of membranes**

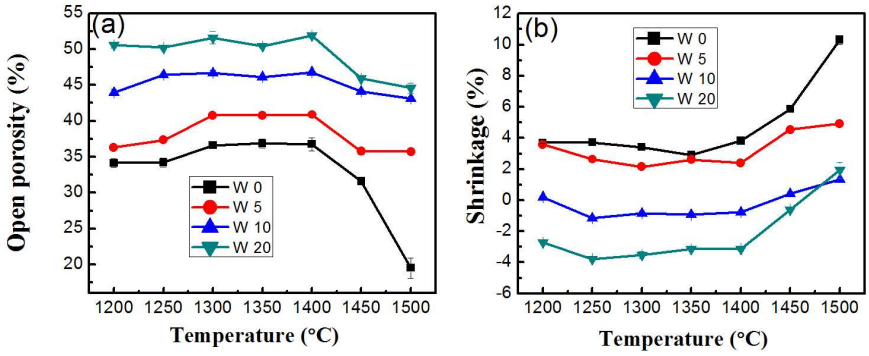


**Fig. S5 (a) Open porosity and (b) shrinkage of the membranes with various $WO_3$ contents (wt. %) at different sintering temperatures.**

Fig. S5 illustrates the effects of $WO_3$ content on the open porosity and linear shrinkage of mullite ceramic membranes with various sintering temperatures from 1200 ˚C to 1500 ˚C. All these samples even with different $WO_3$ contents exhibit similar variation tendency of open porosity as a function of sintering temperature. From 1200 ˚C to 1400 ˚C, they all show an increase in open porosity with sintering temperature, due to a mullitization-crystal-growth induced volume expansion [1], which is opposite as compared to a gradual decrease in open porosity during traditional particulate sintering. The open porosity of the W20 sample could even increase up to as high as 51.9 % at 1400 ˚C. But there is a decrease in open porosity above 1400 ˚C. A significant decrease is observed for the W0 sample when compared with the other samples. A gradual increase in open porosity with $WO_3$ content is observed at all the sintering temperatures ranging from 1200 to 1500 ˚C, which indicates that $WO_3$ could effectively improve the open porosity of ceramic membranes. The percentage shrinkage of all the samples decreases slightly between 1200 and 1300 ˚C, then increases with sintering temperature gradually form 1300 to 1500 ˚C (Fig. S5b). But

the shrinking percentage decreases with increasing $WO_3$ content (from 0 to 20 wt. %), which is consistent with the results of open porosity (Fig. S5a). It can be attributed to the fact that $WO_3$ was favorable to the formation of silica-rich liquid phase, thus promoting the reaction of $Al_2O_3$ and $SiO_2$ and the subsequent anisotropic growth of mullite crystals. Similar positive enhancement of open porosity by using other additives like $V_2O_5$ [5] and $MoO_3$ [6] has also been reported in our previous work.

Tab. S2 summarizes the comparative performance of the ceramic membrane obtained in this work with those reported by other researchers. It can be observed that due to the addition of $WO_3$, the overall performance of ceramic membrane prepared by using fly ash and bauxite in our study is much better than those made by using kaolin, quartz and calcium carbonate in terms of open porosity and flexural strength. Further, by considering additives, the open porosity of ceramic membrane in this work is comparably higher than those with addition of other additives such as MgO and $V_2O_5$. Thus, it is apparent that the performance of ceramic membrane presented in this work is comparably better than that presented in the literature, such as higher open porosity at similar flexural strength.

**Table S2 Comparison of ceramic membrane performance obtained in our work with those available in the literature.**

| Raw materials | Additives | Diameter shrinkage | Open porosity (%) | Flexural strength (MPa) | Mean pore size (μm) | Reference |
|---|---|---|---|---|---|---|
| kaolin, quartz and calcium carbonate | — | 4 % | 30 | 34 | 1.30 | [4] |
| Kaolin, quartz and feldspar | — | — | 44 | 28 | 1.01 | [5] |
| Fly ash and bauxite | MgO | -2~-3 % | 40~45 | 42.74 | 1.89~2.91 | [6] |
| Fly ash and bauxite | $V_2O_5$ | — | 4.15~42.9 | 20~108 | — | [7] |
| Fly ash and bauxite | $WO_3$ | -3.78~1.94 % | 44.58~51.9 | 34.5~87.5 | 0.67~1.78 | This work |

**Results of biaxial flexural strength tests of membranes**

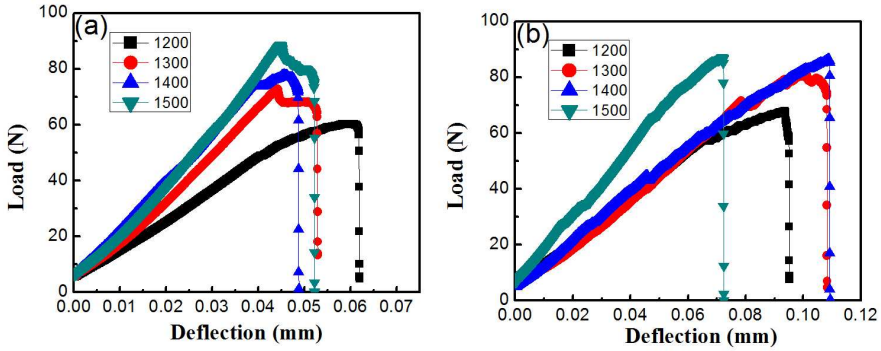


**Fig. S6 Results of biaxial flexural strength tests of the mullite ceramic membranes sintered from 1200 to 1500 °C: (a) typical load-deflection curves of W0, (b) typical load-deflection curves of W20.**

The results of biaxial flexural strength tests of the mullite ceramic membranes are shown in Fig. S6. Fig. S6(a-b) displays the typical load-deflection curves. The curves were plotted by choosing the specimens with strength the closet to the average values. For most of the samples, a nonlinear relationship can be observed between load and deflection before achieving the maximum load, then a rapid degradation is followed.

**SEM images of membranes**

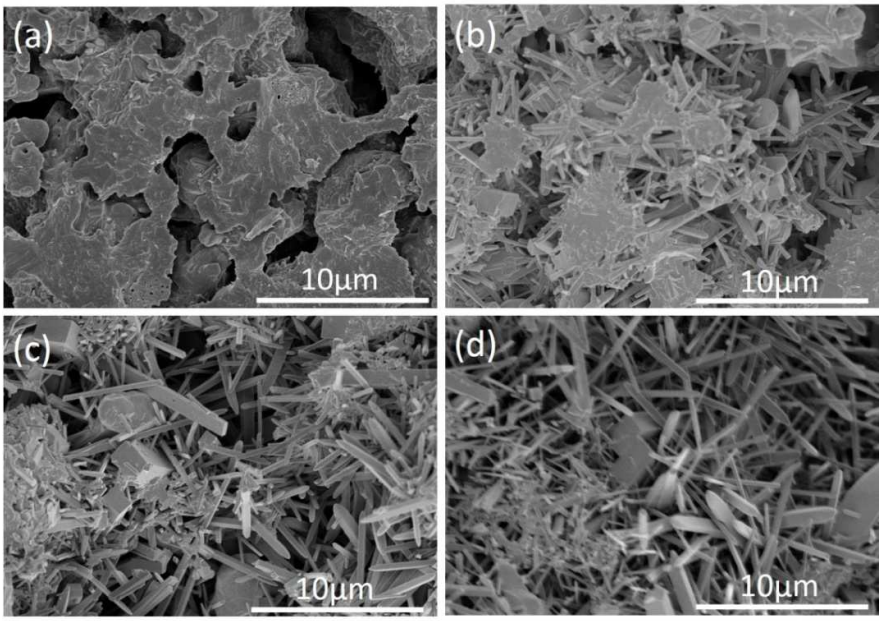


**Fig. S7 Fractured surface SEM images of the sintered mullite membranes (1300 °C for 2 h) with different $WO_3$ contents: (a) 0 wt. %, (b) 5 wt. %, (c) 10 wt. % and (d) 20 wt. %.**

Fig. S7 shows the SEM images of ceramic membranes W0, W5, W10 and W20 sintered at 1300 °C for 2 h. It can be clearly observed that the amount of mullite whiskers was enhanced with the increase in doping level from 0 to 20 wt. %.

**Schematic diagram for oil-in-water emulsion separation**

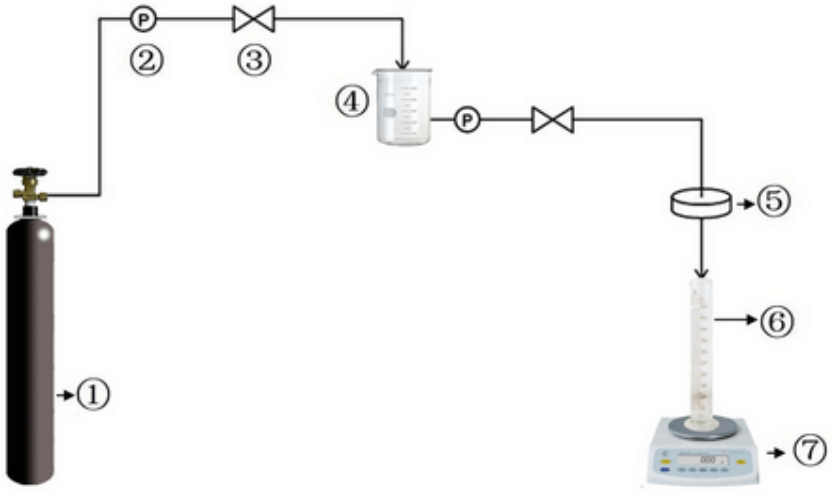


**Fig. S8 Schematic diagram of experimental set-up for oil-in-water emulsion separation using mullite ceramic membrane. ( ① Nitrogen cylinder, ② Manometer, ③valve, ④oil-water emulsion, ⑤ceramic membrane, ⑥test tube, ⑦electronic balance)**

Schematic diagram of experimental set-up for oil-in-water emulsion separation using mullite ceramic membrane is shown in Fig. S8. In the experiment, the nitrogen gas provided the driving force for oil-in-water emulsion separation. The permeate was collected by a measuring cylinder and its weight can be read by electronic balance.

**Oil-in-water emulsion characterization**

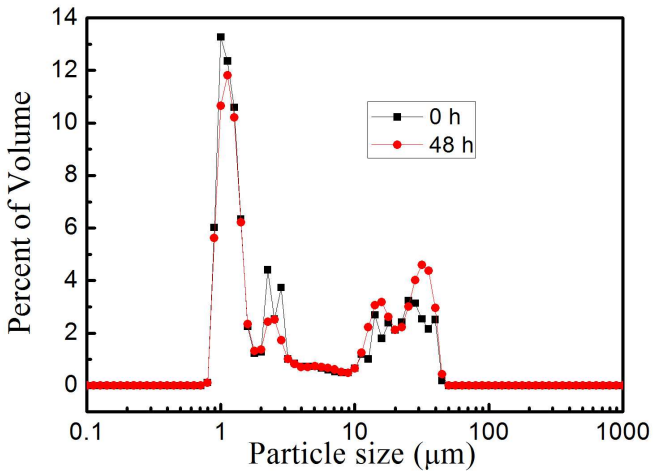


**Fig. S9 Oil droplets size distributions for 48h in oil-in-water emulsion.**

The oil used in this study is machine oil (GL-5, Qiangli). Oil-in-water emulsions were prepared by dissolving a certain amount of machine oil into deionized water with addition of sodium dodecyl sulfate, followed by sonication for 12 h, finally by vigorous magnetic stirring for 48h until they appeared approximately turbid and milky white, indicating good stability and homogeneity. Fig. S9 shows the oil droplets size distributions for 48h in oil-in-water emulsion. As it can be seen, the oil-in-water emulsion is very stable for at least 2 days and the average particle size of oil droplets is 2 μm. Thus, during the one hour filtration, the emulsion could be stable enough for oil droplets removing effectively by ceramic membrane.

**Reference**

1. Chung, F. H., Quantitative interpretation of X-ray diffraction patterns of mixtures. II. Adiabatic principle of X-ray diffraction analysis of mixtures. *J Appl Crystallog* **1974,** *7*, 526-531.

2. Snyder, R. L., The use of reference intensity ratios in X-ray quantitative analysis. *Powder Diffr* **1992,** *7*, (04), 186-193.

3. Cao, J.; Dong, X.; Li, L.; Dong, Y.; Hampshire, S., Recycling of waste fly ash for production of porous mullite ceramic membrane supports with increased porosity. *J Eur Ceram Soc* **2014,** *34*, (13), 3181-3194.

4. Dong, Y.; Hampshire, S.; Zhou, J.-e.; Ji, Z.; Wang, J.; Meng, G., Sintering and characterization of flyash-based mullite with MgO addition. *J Eur Ceram Soc* **2011,** *31*, (5), 687-695.

5. Li, J.-H.; Ma, H.-W.; Huang, W.-H., Effect of $V_2O_5$ on the properties of mullite ceramics synthesized from high-aluminum fly ash and bauxite. *J Hazard Mater* **2009,** *166*, (2–3), 1535-1539.

6. Zhu, L.; Dong, Y.; Hampshire, S.; Cerneaux, S.; Winnubst, L., Waste-to-resource preparation of a porous ceramic membrane support featuring elongated mullite whiskers with enhanced porosity and permeance. *J Eur Ceram Soc* **2015,** *35*, (2), 711-721.